Novel rapid shutdown strategies for runaway electron suppression in DIII-D

2011 Nucl. Fusion 51 103001

(http://iopscience.iop.org/0029-5515/51/10/103001)

IOP Publishing and International Atomic Energy Agency Nuclear Fusion
Nucl. Fusion **51** (2011) 103001 (9pp) doi:10.1088/0029-5515/51/10/103001

Novel rapid shutdown strategies for runaway electron suppression in DIII-D

N. Commaux[1], L.R. Baylor[1], S.K. Combs[1], N.W. Eidietis[2], T.E. Evans[2], C.R. Foust[1], E.M. Hollmann[3], D.A. Humphreys[2], V.A. Izzo[3], A.N. James[3], T.C. Jernigan[1], S.J. Meitner[1], P.B. Parks[2], J.C. Wesley[2] and J.H. Yu[3]

[1] Oak Ridge National Laboratory, Oak Ridge, TN, USA
[2] General Atomics, PO Box 85608, San Diego, CA 92186-5608, USA
[3] University of California-San Diego, La Jolla, CA, USA

Received 21 January 2011, accepted for publication 6 May 2011
Published 16 August 2011
Online at stacks.iop.org/NF/51/103001

Abstract
New rapid shutdown strategies have been recently tested in the DIII-D tokamak to mitigate runaway electrons (REs). Disruptions in ITER are predicted to generate multi-MeV REs that could damage the machine. The RE population in large tokamaks is expected to be dominated by avalanche amplification which can be mitigated at high density levels by collisional drag. Particle injection schemes for collisional suppression of RE have been developed and tested in ITER-relevant scenarios: massive gas injection, shattered pellet injection (SPI) and shell pellet injection. The results show an improved penetration of particles injected with the SPI. Another strategy has been developed to harmlessly deconfine REs by applying a non-axisymmetric magnetic perturbation to worsen their confinement. This technique appeared to deconfine seed RE before the avalanche process could amplify the RE beam. The last method tested was to use the plasma position control system on the RE beam to prevent it from contacting the wall. This proved effective in preventing high current RE beam from touching the wall and providing more time to mitigate an existing RE beam but a successful 'soft landing' (without fast final losses) of the RE has not been observed yet.

(Some figures in this article are in colour only in the electronic version)

1. Introduction

Prevention and mitigation of the harmful effects from disruptions are essential for reliable operation of ITER. One of the potentially most harmful effects from a disruption is the generation of runaway electrons (REs). These high energies (tens of MeV) and high currents (several mega-ampere) focused electron beams [1] can damage elements of the first wall if they strike and penetrate the material surfaces. Thus three new rapid shutdown strategies employing different mechanisms have been recently tested in the DIII-D tokamak to mitigate RE. The first one is the collisional suppression of RE. The second strategy is the position control of the RE beam in order to prevent contact with the walls. The third strategy is the magnetic deconfinement of the RE.

The collisional suppression of the RE is currently one of the most commonly tested strategies. It consists of rapidly increasing the electron density up to a critical value n_{crit} [2] where collisional drag suppresses the RE. This is done by injecting massive (relative to the plasma particle content) amounts of impurities. The 'usual' method known as massive gas injection (MGI) consists of injecting a significant amount of gas (several 100 Pa m^3 in DIII-D) through fast valves. The DIII-D MGI system consists of an array of six fast solenoid valves [3] allowing a faster delivery of a much more significant amount of impurities compared with the more common single valve design [4, 5]. In addition, two new techniques were developed and tested recently on DIII-D: shattered pellet injection (SPI) and shell pellet injection (SHPI). These techniques were tested in an ITER-relevant scenario: lower single-null ELMing H-mode plasmas. In several cases, the thermal energy content W_{th} of the plasma was scanned by changing the injected neutral beam power (0–14.5 MW) to test if the amount of thermal energy available in the plasma could have an influence on the ionization fraction and the ablation rate (for SPI and SHPI). Figure 1(*a*) shows the plasma configuration used for these experiments as well as the geometry of the different massive particle injection systems.

The second strategy tested is to control the position of an existing RE beam to prevent contacts between the high current RE beam and the vacuum vessel first wall. This technique was applied using the position control and shaping coils of DIII-D in order to prevent the RE beam from crashing on the first wall. The main goal of this technique is to increase the time available to apply other mitigation techniques.

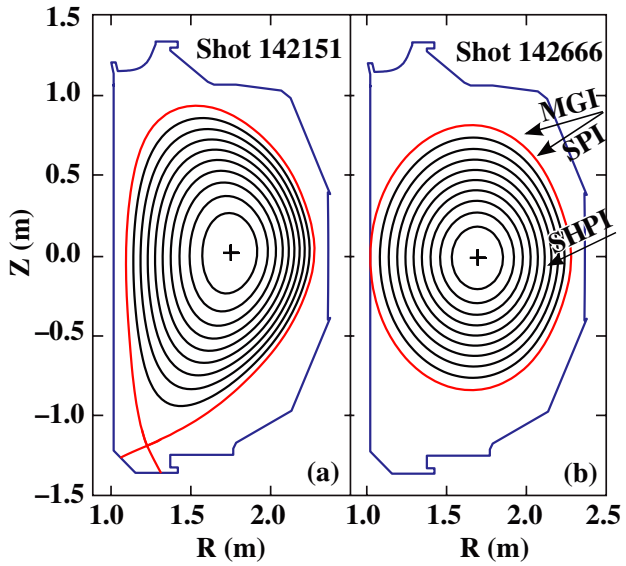

Figure 1. Equilibrium reconstruction of poloidal flux contours for the scenarios used (*a*) for massive particle injection experiments; (*b*) to generate significant RE currents. (Also shown is the geometry of MGI, SPI and SHPI.)

Resonant magnetic perturbation (RMP) was the last strategy tested on DIII-D to lower the confinement of RE to prevent the formation of a significant RE beam. This technique (which had already been tested with some success on TEXTOR [6] and JT-60U [7] with $n = 1$ and $n = 2$ fields) was applied on DIII-D using in-vessel coils in order to generate an $n = 3$ or $n = 1$ non-axisymmetric magnetic field on plasmas prone to generate significant amounts of RE. RMP and feedback control were tested on DIII-D on discharges producing reliably significant RE population using symmetric, limited, low elongation ($\kappa = 1.3$–1.4) target plasmas (as shown in figure 1(*b*)) heated by electron cyclotron heating (2 MW) and terminated by an argon pellet, so the runaway beam naturally forms near the mid-plane. These RE beams had a random initial amplitude in the 100–600 kA range and an average energy of ∼20 MeV [8]. The amplitude of the runaway current and its duration is heuristically calculated by subtracting to the measured current a hypothetical resistive L/R exponential decay normally observed when no significant RE channel is formed and the plasma is essentially thermal. These three different strategies could potentially be compatible with each other and employed simultaneously or in sequence during a fast shutdown.

2. Collisional suppression

In order to obtain collisional suppression of RE, the total electron density (free and bound) must be increased up to levels above a critical value n_{crit}. This value is estimated using a 0D calculation of the toroidal electric field generated during current quench (CQ) by the plasma current decay. This calculation uses the formula for the critical electric field $E_c \sim 0.05\ (2n_e + n_{bound})$ where E_c is the critical field (in V m^{-1}) below which the toroidal electric field is not sufficient to generate the avalanche process, n_e the free electron density and n_{bound} the bound electron density (in 10^{20} m^{-3}). The toroidal electric field E_{tor} during the CQ is calculated using $E_{tor} = L(\mathrm{d}I_p/\mathrm{d}t)$ with I_p the plasma current and L the self-inductance of the plasma assumed to be equal to the pre-disruption value calculated using equilibrium reconstruction. In the fastest plasma current decay cases in DIII-D, E_{tor} appears to be of the order of 50 V m^{-1}. Assuming that $n_{bound} \ll n_e$ in these deuterium injection cases (since the electron temperature during the thermal quench (TQ) is measured by spectroscopy at several electron volts), $n_e \sim n_{crit}$ when $E_{tor} = E_c$. Then n_{crit} can be estimated at $\sim 5 \times 10^{22}$ m^{-3}. Three rapid particle delivery techniques have been tested on DIII-D: MGI, SPI and SHPI. Measuring local densities on such short time scale (less than 1 ms) and density levels (several 10^{21} m^{-3} on average) proved very challenging. Thus these techniques were evaluated using the measurement of the total number of free electrons in the discharge as a metric characterizing their efficiency at increasing the total electron density (free + bound) towards n_{crit}.

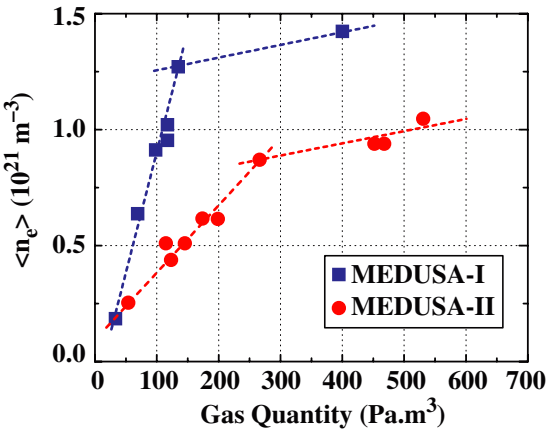

Figure 2. Density perturbation induced by MGI as a function of the injected gas quantity for the 2 MGI valve configurations: open duct MEDUSA-I and restricted duct MEDUSA-II.

2.1. Massive gas injection

The MGI consists of injecting massive quantities of gas through fast valves. This method was tested on DIII-D using the six fast-valve array MEDUSA [3]. A modified version of the original MEDUSA-I injector was used to conduct a systematic injected gas quantity (Q) and target plasma thermal energy variation experiment with helium MGI. This modified MEDUSA-II injector was modified in order to implement the new SPI injector at the same location. Thus this injector feeds the gas through a 1.3 m long coaxial duct supporting the SPI breaker plate described in section 2.2. The restricted duct in front of the MEDUSA-II injector was observed to have a detrimental effect on the assimilation fraction $f_{assim} = N_{He}^{2+}/N_{He} = N_e/2N_{He}$ of the MGI system. N_e, N_{He} and N_{He}^{2+} are the total in plasma-free electron number, the total injected He number and the corresponding in plasma fully ionized He number. f_{assim} dropped from ∼0.3 with MEDUSA-I down to ∼0.15 for MEDUSA-II. Figure 2 shows that the density perturbation induced by MGI as measured by interferometry dropped by a factor of 2 with the MEDUSA-II configuration. The phenomenon that could explain this difference is the lower gas conductance of the annular duct and the presence of the

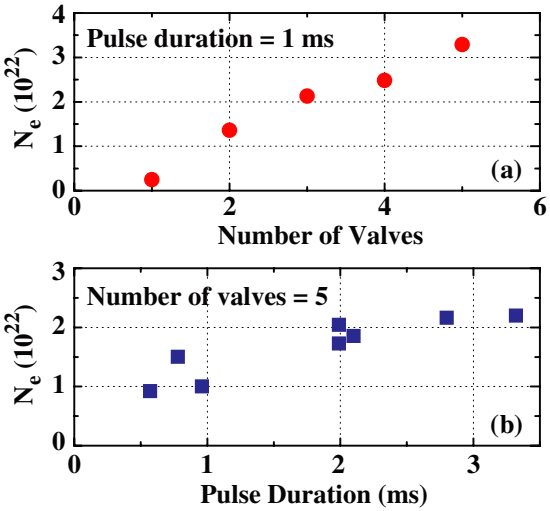

Figure 3. Maximum number of electrons obtained in the discharge after an MGI He injection as a function of (*a*) the number of valves actuated (pulse duration constant) using MEDUSA-I and (*b*) the pulse duration (number of valves actuated constant) using MEDUSA-II.

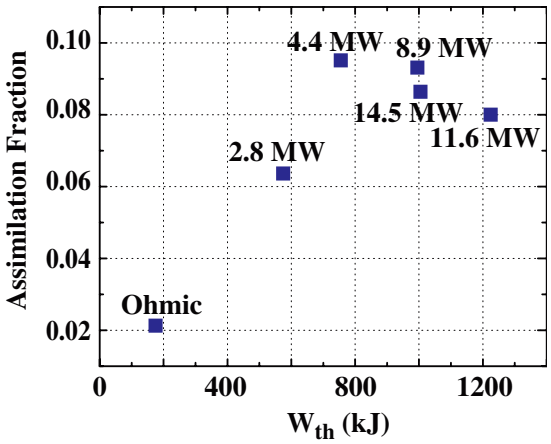

Figure 4. Assimilation fraction as a function of the thermal energy content of the discharge for MGI (330 Pa m^3 of He: 6 valves with a pulse width of 2.1 ms).

breaker plate of the SPI partially obstructing the outlet of the duct. The elements could force the gas pulse from MEDUSA to become wider both in time and spatially inducing a lower gas pressure at the interface plasma/MGI gas jet. This explanation is supported by the results of Q scans with constant plasma conditions. Figure 3 summarizes the results obtained by increasing the valve pulse duration or by changing the number of valves injecting simultaneously. Figure 3(*a*) shows that with a short 1 ms pulse duration, increasing Q (30–130 Pa m^3) by increasing the number of valves operated with MEDUSA-I, the assimilation fraction remains constant since N_e increases linearly with the number of valves. In contrast figure 3(*b*) shows that with a fixed number of valves, increasing Q by increasing the pulse duration (in MEDUSA-II) is not as efficient: N_e appears to saturate for a pulse duration above 1.5–2 ms. The absolute N_e values should not be compared directly between these two sets of data since the set shown in figure 3(*a*) was produced using the former and more efficient MEDUSA-I configuration and the one shown in figure 3(*b*) was produced using MEDUSA-II. But the trends show that in the Q range tested here, the assimilation fraction is not simply dependent on Q but also on the duration of the injection. This critical time of 1.5–2 ms appears to be correlated with the time delay between the time the gas pressure front hits the plasma and the time of the TQ onset [9]. This could be interpreted as the fact that the plasma can assimilate and ionize the gas as long as there is significant thermal energy available in the plasma since this energy is lost rapidly after the TQ onset. To test directly the influence of the thermal energy content, a thermal energy scan was thus achieved on DIII-D by changing the neutral beam input power from 0 (ohmic) to 15 MW and injecting a constant helium Q (330 Pa m^3 of helium with both six valves actuated and the same pulse duration of 2.1 ms). The results of this thermal energy scan are shown in figure 4. This figure shows that the thermal energy clearly has an effect for low injected power (up to 5 MW) and low thermal energy content with a strong increase in f_{assim}. Beyond this value, f_{assim} saturates at ∼0.09. This saturation could be due to the fact that the favourable higher thermal energy content is compensated by a possible stronger MHD activity triggering a faster loss of the plasma energy thus reducing the time available to assimilate the injected particles. These data show that MGI efficiency relies on fast delivery of the particles linked with a short valve pulse duration and high conductivity of the gas duct. It shows also that the thermal energy content can improve this fraction up to a certain limit probably linked with MHD activity.

2.2. *Shattered pellet injection*

The SPI technique consists of the injection of a large cylindrical cryogenic pellet (diameter: 15 diameter and length: 20 mm on DIII-D). Before entering the plasma, the pellet is shattered into submillimetre fragments by impacting on two metal breaker plates. Shattering the pellet increases surface area (3–4 times according bench tests) for a more efficient ablation (according to preliminary 1D calculations) and protects the first wall from possible damage by impact from an intact pellet. The DIII-D SPI system [10] injects enough particles into the plasma to reach an average electron density close to n_{crit} [11]. Experiments were carried out using the SPI technique to successfully terminate six discharges. The plasma conditions in these discharges were a toroidal field of 2.1 T, plasma current of 1.5 MA and neutral beam injection power of 0–13.4 MW. The pellets injected in these discharges were deuterium pellets injected with a speed range 500–600 m s^{-1} and contained ∼1.9×10^{23} atoms (400 Pa m^3). Local densities were determined using the visible bremsstrahlung emission of the plasma measured with several visible spectrometers. These measurements taken at different toroidal locations enabled a lower bound estimate (because of signal saturation) of the total number of electrons N_e in the discharge during the disruption and thus the assimilation fraction. As in the MGI case, a thermal scan enabled testing the influence of the thermal energy content of the plasma on the assimilation fraction. The results of this scan are shown in figure 5. This assimilation fraction appears to increase weakly with the thermal energy content of the discharge for the NBI heated discharges (the assimilation

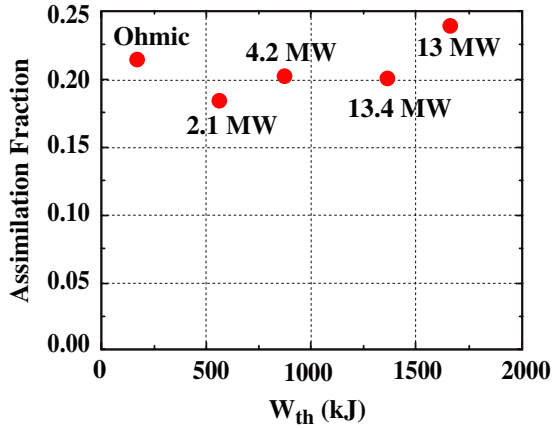

Figure 5. Assimilation fraction as a function of the thermal energy content of the discharge for SPI (400 Pa m^3 of D_2).

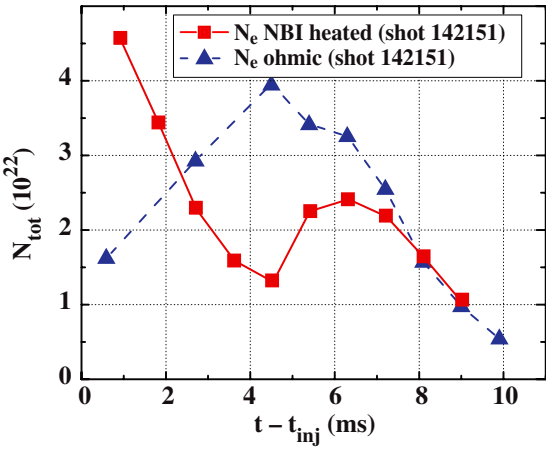

Figure 6. N_e during SPI induced shutdowns of an ohmic shot and high power (15 MW) NBI heated shot.

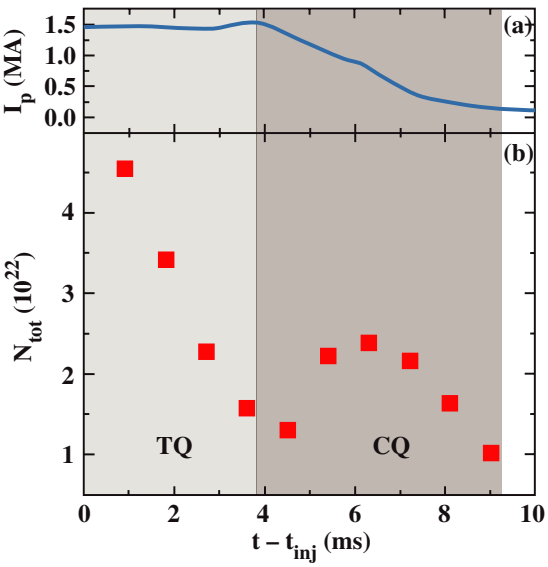

Figure 7. Plasma current (*a*) and N_e (*b*) during an SPI-induced shutdown (shot 142151) with thermal energy content of 1600 kJ (t_{inj} being the injection time). The light shaded area shows the TQ phase and the dark shaded the CQ phase.

fraction varying between 18% and 24% for thermal energy content varying between 172 and 1660 kJ). The ohmic case seems to be an exception: the assimilation process appears to be longer thus improving the assimilation when compared with a weakly heated discharge. Figure 6 shows a comparison of N_e for an NBI heated shot and an ohmic shot. The increase in N_e (thus the assimilation) lasts ~5 ms versus less than 1 for the NBI heated case. A typical example of the time evolution of N_e after the SPI injection occurred at $t = t_{inj}$ on an NBI heated shot during the induced fast shutdown is shown in figure 7. This figure shows first that the maximum N_e value is $\sim 4.5 \times 10^{22}$ electrons, which indicates a 24% assimilation fraction during this SPI induced shutdown. Figure 7 shows that N_e varies significantly during the fast shutdown: it decays very fast during the TQ, but starts to increase again after the onset of the CQ. The fast decrease during the TQ can be explained by the cooling of the plasma lowering the ionization rate, but not why it increases at the beginning of the CQ. Since the heating power is rather constant during this phase, the fact that N_e increases could indicate a heat or particle transport effect or a recycling effect. Simulations of these results with the 3D MHD code NIMROD [12] have been carried out. The SPI injection was simulated by a homogeneous deposition of the particle content of the pellet (flat density profile at $t = t_{inj}$). The results from the simulations show that a change in the heat confinement could be responsible for the increase in N_e at the onset of the CQ. Figure 8 shows that at the onset of the CQ ($t = t_{inj} = 5$ ms in the simulation), the ergodization of the magnetic surfaces by the major MHD activity (dominated by $n = 1$) induces a loss of heat confinement in the centre of the plasma ($\rho < 0.7$). The heat is transported rapidly along the ergodized field lines towards the edge ($\rho > 0.7$) and thus reheats the neutrals localized at the edge. The average electron temperature at the edge increases from ~1 to ~5 eV as shown in figure 8(*a*). This is enough to increase the ionization fraction of the deuterium locally from ~0.01 to ~0.99 which provides a very significant amount of free electrons in the discharge. This is assuming ionization/recombination equilibrium. The density increase after the onset of the CQ calculated by NIMROD and shown in figure 9 is consistent with the experimental results though the simulation predicts this increase earlier in the TQ phase. Since NIMROD does not take into account the recycling, this simulation cannot show if the changes in the recycling rate due to the increased temperature of the wall (radiation and conducted heat to the walls) could contribute to this increase of N_e by the release of significant amounts of deuterium and carbon impurities.

The experiments carried out recently on DIII-D provided also for the first time a direct comparison between the MGI (using the MEDUSA-II configuration since the MEDUSA-I was not available anymore) and SPI techniques using the same plasma target, very similar injection geometries as shown in figure 1(*b*), the same injected species and the same amount of particles. Figure 10 shows the line integrated density during an ohmic plasma rapid shutdown using comparable MGI and SPI (400 Pa m^3 of D_2 in both cases applied on the same plasma scenario). Since the central interferometry chord is located at a toroidal location 150° apart from the injection location, this density measurement shows the particles that have already been transported and homogenized in the plasma.

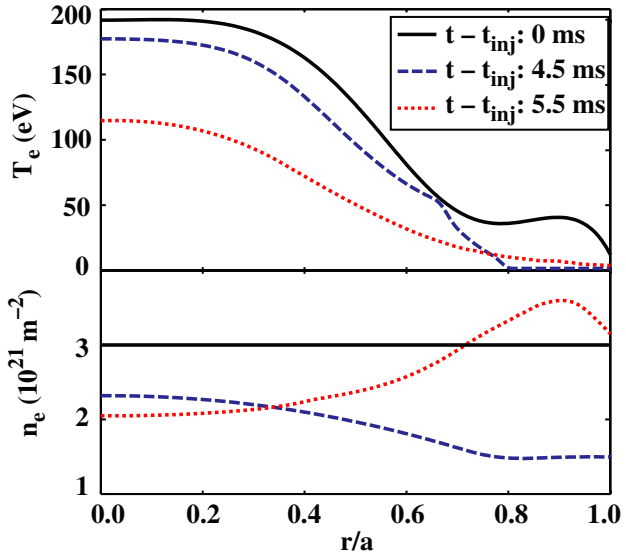

Figure 8. Electron temperature (*a*) and density (*b*) profiles calculated by NIMROD at the beginning of the simulation ($t = 0$) based on shot 142151, before the onset of the CQ ($t - t_{\rm inj} = 4.5$ ms), and after the onset of the CQ ($t - t_{\rm inj} = 5.5$ ms).

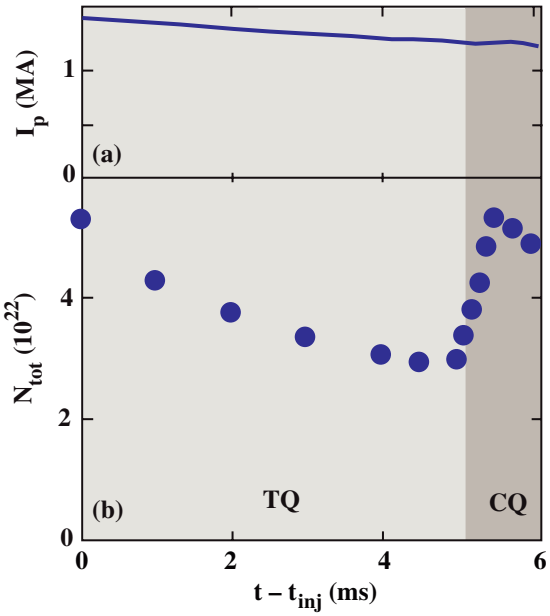

Figure 9. Plasma current decay (*a*) and total number of free electrons in the plasma as a function of time (*b*) calculated by NIMROD simulating a SPI during shot 142151.

The maximum line integral density in the SPI case is twice as high as the maximum MGI density. The assimilation fraction is thus ∼15% for MGI compared with ∼25% for the SPI. The timing of the homogenization process is also more favourable for SPI (maximum assimilation and total homogenization observed ∼3 ms after the injection). The SPI reaches the maximum density when the plasma current is 80% of its initial value (maximum assimilation and total homogenization observed ∼10 ms after the injection). The MGI case reaches its maximum density when the plasma current is reduced 40% from its initial current. The fact that MEDUSA-II was used for these tests has to be taken into account though. It is possible

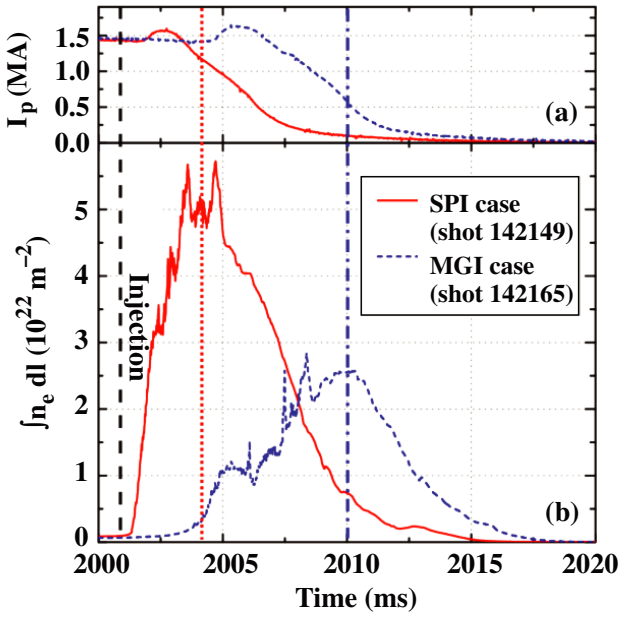

Figure 10. Plasma current (*a*) and line integrated density (*b*) during SPI (solid) and MGI (dashed) rapid shutdown of an ohmic plasmas as a function of time. The vertical lines show the time when the density starts to roll-over for the SPI (dot) and MGI (dashed–dotted).

that the results would have been closer using the more optimal MEDUSA-I configuration. This faster rise of the density for the SPI all around the torus may improve the efficiency of the collisional mitigation since the particles are delivered when the toroidal electric field is at its maximum early in the avalanche multiplication phase. This faster rise of the density could indicate different transport mechanisms. The SPI would rely on parallel transport in the core plasma since it appears to penetrate much deeper than MGI that stays at the edge as colder and slower neutrals then mix with the plasma due to MHD events during the CQ [13].

2.3. Shell pellet injection

The SHPI basic principle is to fire a solid shell containing a dispersive payload at the plasma. The hard shell of this pellet is ablated by the plasma as it transits through it. When reaching the plasma core, the shell is expected to break open, releasing the payload throughout the core region. This impurity payload is expected to provide enough electrons to the core to reach $n_{\rm crit}$. Two different types of dispersive payloads have been tested: dust grains or high-pressure gas [14]. Proof-of-principle shell pellets were tested on DIII-D using small (outer diameter ∼ 2 mm, wall thickness ∼ 0.4 mm) polystyrene spherical shells filled with either pressurized (10 bar) argon gas or with boron powder [15]. The pellets were fired at an initial velocity $v \approx 350\ {\rm m\,s^{-1}}$ at the plasma core. These small shell pellets did not disrupt the plasma and penetrated in to normalized minor radius $r/a \approx 0.5$ before breaking open and dispersing their payload. The payload release, ionization and rapid (within about 10 ms) dispersion through the core were confirmed and studied using fast framing visible camera imaging, charge-exchange recombination and UV spectroscopy. Following this successful demonstration, large shell pellet experiments were attempted in 2009. In these experiments, much larger

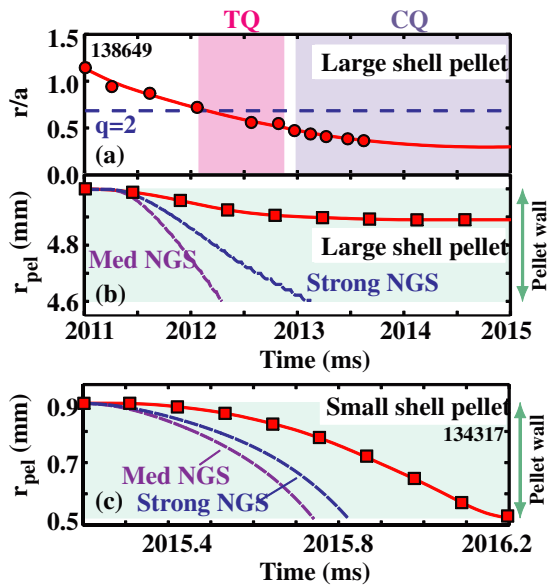

Figure 11. (*a*) Pellet trajectory r/a as a function of time for a large shell pellet. Experimental (solid) and calculated using two different NGS models (dash) burn-through of a large (*b*) and small (*c*) shell as a function of time (the thickness of the pellet shell is shown by the vertical arrows on (*b*) and (*c*)). (Adapted and reprinted with permission from [14]. Copyright 2010 by the American Institute of Physics.)

polystyrene shells (outer diameter $\approx$ 1 cm, wall thickness $\approx$ 0.4 mm) filled with boron powder were fired at velocity $v \approx 200\,\mathrm{m\,s^{-1}}$ through the plasma core. These bigger shells have enough volume to carry enough payload to reach ideally densities close to n_{crit} (several $10^{22}\,\mathrm{m^{-3}}$). During the experiments, these large shell pellets shut down the discharge and initiated the TQ but without breaking open in the plasma. Figure 11 shows a pellet radial trajectory for a big shell and shell wall burn-through of a large and small shell pellet. The pellet trajectory is estimated from fast camera data while burn-through is estimated by assuming that pellet ablation rate is proportional to ablation plume brightness, with a normalization of mass ablated obtained using total observed electron density rise from interferometers. Figure 11(*a*) shows the large shell pellet position (r/a) as a function of time—its position at the moment it triggers the TQ is consistent with the $q = 2$ surface. The curve in figure 11(*a*) is due to the pellet trajectory missing the plasma magnetic axis (as shown in figure 1). Figure 11(*b*) shows burn-through of the pellet walls as a function of time for a large shell pellet. From this figure, it is apparent that the large shell pellet wall is estimated to have ablated only 25% of its shell thickness. After $t \approx 2013$ ms (end of the TQ), ablation effectively turns off since the plasma temperature is now too low. After that the large shell pellet passes through the rest of the plasma unperturbed. Figure 11(*b*) also shows estimates of the polystyrene shell ablation predicted from ablation models derived from fuelling deuterium pellet ablation models adapted for polystyrene. The models shown here are 'med NGS'—a neutral gas shielding ablation model which does not include electrostatic shielding and 'strong NGS' a similar model including electrostatic shielding. Overall, both models do a reasonably good job of predicting the small shell pellet ablation as shown in figure 11(*c*), but are optimistic at predicting large shell pellet ablation. This discrepancy could arise from pre-cooling (anomalous heat transport at the strongly perturbing large pellet cold front). These results show the shell has to break open before reaching the $q = 2$ surface (since the TQ starts at that point and effectively shut down the ablation processes) thus the wall thickness of the shell should be reduced to 0.1 mm on DIII-D. Recently, new spherical polystyrene shells were developed using inertial fusion target technology consisting of a 1 cm outer diameter and a 0.1 mm wall thickness. These new spherical polystyrene shells will be tested during the 2011 campaign on DIII-D.

3. Active feedback control of the runaway beam

A robust defense against the destructive effects of the RE beams requires multiple layers of protection. Should the collisional suppression mitigation methods described above fail to prevent the formation of a runaway beam, active position control can prevent the beam from colliding with the wall. Controlling the amplitude of the runaway current would provide an opportunity for slow time-scale mitigation techniques or natural decay processes to gradually terminate the runway beam without significant damage to the PFCs.

DIII-D typically utilizes a real-time EFIT (rtEFIT) equilibrium reconstruction coupled with an Isoflux control algorithm [16] for plasma boundary control. However, rtEFIT is unreliable in producing converged equilibrium reconstructions during the rapid transients of the CQ phase. This results in a loss of Isoflux boundary control during the CQ. An alternate control algorithm that utilizes linear estimators of the plasma radial and vertical position has been observed to be more robust to the transients during and immediately after the CQ. This algorithm is activated at the start of the CQ to allow for active feedback control of the runaway beam position.

The first control challenge posed by a runaway beam is to re-establish radial equilibrium immediately after CQ. The outer poloidal coils that are primarily responsible for radial equilibrium on DIII-D are not capable of slewing rapidly enough towards zero current to maintain radial equilibrium during the 5–10 ms CQ. Without corrective measures, the runaway beam compresses against the inner wall and, typically within 30–50 ms, terminates in a disruption without a significant loss of RE beam current. In order to avoid this compression, the inner wall poloidal coils are given saturated commands at the start of CQ to push the plasma off the wall, while at the same time the outer coil currents are reduced as rapidly as possible. Depending upon the level of RE flattop current, the effort to push the plasma off the inner wall can result in a RE beam with diverted topology. RE beam lasting more than 150 ms (an example is shown in figure 12) has been achieved using this control method. Vertical stability of the runaway beam is maintained using standard derivative control. Feedback controlled movement of the beam both above and below the mid-plane has been demonstrated, as shown in figure 13. Although the initial runaway beam is typically circular and vertically stable, vertical control is maintained even if the beam becomes elongated and diverted by the radial control. Achieving a reliable radial position control has proven to be more challenging. A successful 'soft landing', wherein the RE current decays completely without

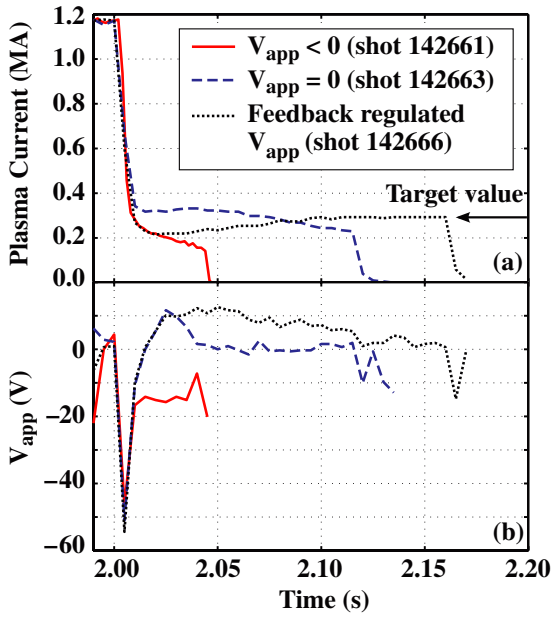

Figure 12. RE current (a) evolution for a different applied loop voltage V_{app} (b) as a function of time: negative (solid), zero (dashed) and feedback regulated (dotted) at $I_{RE} = 300$ kA.

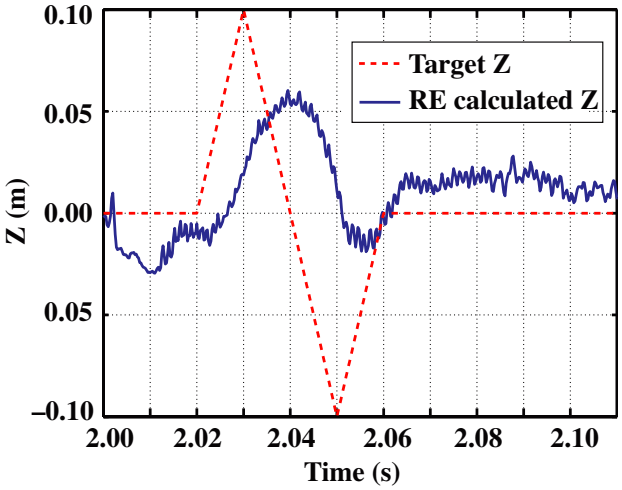

Figure 13. Vertical position feedback control of the RE beam produced during shot 142672: vertical position of the magnetic axis of the plasma using magnetic reconstruction (solid) compared with the target value (dash).

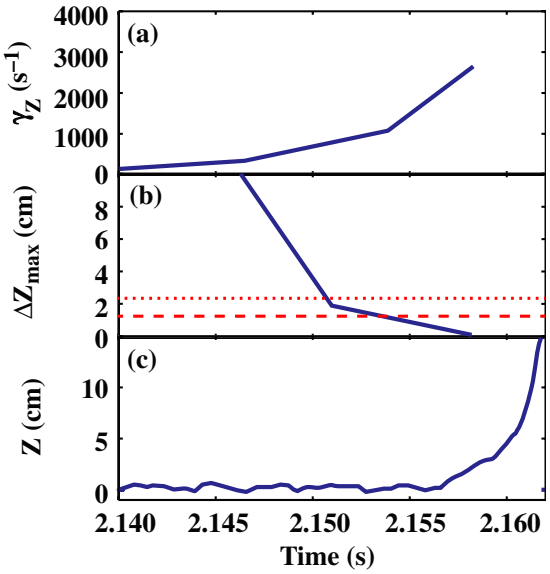

Figure 14. Evolution of calculated controllability in shot 142666 during the RE plateau phase as a function of time: (a) vertical growth rate γ_Z, (b) maximum controllable displacement ΔZ_{MAX}, (solid), control limit with noise only (dotted), control limit with noise plus disturbance (dashed) (c) vertical position.

any vertical displacement event (VDE) or other disruption, has not yet been observed. Although the RE position can be held steady for long periods of time, all of the extended runaway plateaus produced in DIII-D appear to terminate in a sudden loss of RE (as shown in figure 12) following growth of an MHD instability. The RE lost in these sudden events appear to convert their current to thermal current, which then decays on approximately the same L/R time scale seen in the original CQ (see figure 12). In the case of the longest plateaus produced, corresponding to plasmas pushed off the inboard wall and diverted, as well as high positive applied loop voltage, the instability is a VDE as the controllability boundary is crossed. The vertical controllability of a plasma is well-described by the maximum controllable displacement, a metric that quantifies the control capability of the control system relative to a given plasma equilibrium. When the maximum controllable displacement falls below a critical value (typically set by the background noise level or amplitude of unavoidable disturbances such as ELMs or locked modes), vertical control is lost and a VDE occurs [17]. Figure 14 shows the change in controllability as a function of time near the end of the runaway plateau in discharge 142666. The growth rate γ increases rapidly, while the maximum controllability ΔZ_{MAX} decreases. The dotted line denotes the control boundary at which DIII-D plasmas are stable in the presence of noise alone, but can be lost by various kinds of disturbances. The dashed line represents the absolute control boundary for DIII-D, below which a VDE is guaranteed due to the typical background noise amplitude. The final equilibrium (shown in figure 15) is uncontrollable because of sufficiently high elongation ($\kappa \sim 1.65$) and high internal inductance ($\ell_i \sim 2$), as well as poor coupling to the stabilizing wall.

The ideal scenario for control of RE would drop the elongation and produce an inboard wall-limited low elongation equilibrium early in the RE plateau phase. Regulation of the radial and vertical position of such a RE channel would enable slow deconfinement via limited collisional loss or controlled scraping against an armoured inboard wall surface. In the absence of sufficient radial control, the plasma will continue to move inward major radially, and potentially deconfine the runaways rapidly in a localized region, increasing the chance of damage. A loss rate that is faster than the PF coils' capability for vertical field variation will produce such an uncontrolled radial loss. RE discharges in DIII-D with plateau phases <50 ms in duration tend to be examples of such uncontrolled radial motion, possibly due to incompatibility of the radial control algorithm feedback gains with what is required by RE dynamics. Such discharges appear to terminate in kink-like instabilities prior to any vertical motion, consistent with

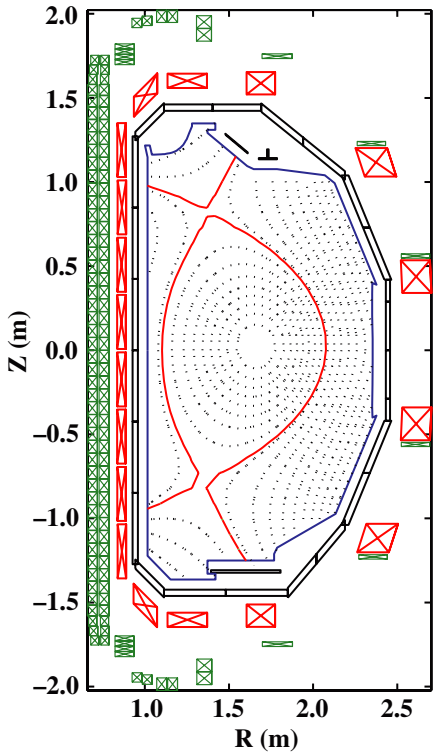

Figure 15. Equilibrium reconstruction (from rtEFIT) during the RE plateau phase of shot 142666 immediately before the onset of the VDE showing an elongated equilibrium ($\kappa \sim 1.65$).

being inboard wall-limited and nearly circular. A reduction in minor radius corresponding to inward motion would tend to decrease internal inductance and edge safety factor and produce a current-driven global kink mode in a thermal plasma. We speculate that similar instability dynamics govern the loss of the RE channel in these cases as well. Avoiding such VDEs and achieving a 'soft landing' will be the focus of future RE control studies.

In addition to position control, the ability to sustain a RE current channel long enough to apply slow deconfinement techniques requires control of the RE current amplitude itself. Recent experiments in DIII-D have demonstrated that applied loop voltage V_{loop} can strongly affect the RE current amplitude, and that real-time feedback can regulate this amplitude to a desired level while the current channel persists. This capability allowed substantial increase in the duration of the RE current plateau in DIII-D from ~20 ms typical of unregulated RE currents in previous experiments up to >150 ms with regulation. Figure 12 compares discharges in which the applied V_{loop} was negative, zero, and feedback regulated to drive the RE current to 300 kA control target value. It shows a clear influence of the V_{loop} on the runaway current amplitude and that an effective feedback control on the runaway amplitude can be achieved. Further studies will examine the relation between the observed RE growth rate using this technique and the internal electric field.

4. Magnetic deconfinement of REs

A seed population of high energy electrons can avalanche to convert a large fraction of the thermal plasma current to relativistic current. The dynamics of this process imply that for sufficiently high V_{loop} assumed to be produced by the plasma current decay, the final runaway current I_{RE} is related to the initial seed current I_{SEED} via $I_{\text{RE}} \sim I_{\text{SEED}} e^G$, where $G \approx I_{\text{p}}/(I_{\text{A}} \ln \Lambda)$, and $I_{\text{A}} \approx 0.02\ 0.02$ MA [2]. For typical DIII-D disruption experiments, the seed amplification e^G is on the order of 20–50, so that the final runaway current value depends strongly on the size of the initial seed population. Under this relatively low-gain condition, the size of the seed can provide a strong mechanism for limiting the final runaway current value by reducing the magnitude of the seed. In addition to collisional damping, reduction of either seed or avalanched RE populations (and current) can be achieved through their deconfinement on open field lines [18]. This phenomenon occurs naturally during the TQ because of the violent MHD events that characterize the TQ [7]. These instabilities typically produce a near-total loss of thermal energy on time scales much shorter than possible with cross-field transport, implying a combination of radiation and parallel transport [19]. These open field lines can also deconfine RE that precede the TQ (seeds) or are generated in the TQ. Another form of RE deconfinement due to magnetic field configuration perturbed from the axisymmetric target equilibrium has been demonstrated in several devices (TEXTOR, JT-60U) using externally applied non-axisymmetric fields [6, 7]. Recent experiments in DIII-D have studied this effect by applying $n = 3$ and $n = 1$ fields using in-vessel coils. Either $n = 3$ or $n = 1$ fields up to 80 G at the plasma surface were applied to Ar pellet-induced disruptions in limited or diverted plasma configurations. Diverted plasmas have been observed to produce RE current channels with lower probability in DIII-D, while limited (lower elongation) equilibria produce RE current with high probability. Application of $n = 3$ RMP fields prior to onset of the TQ may suppress the post-disruption RE current in both cases, with apparently higher effectiveness in diverted plasmas. Figure 16 summarizes the statistics for both configurations. No diverted cases were observed to have visible RE current with $n = 3$ fields applied (before the TQ), and a ~50% reduction in incidence of post-disruption RE current was observed with limited plasmas. In contrast to the significant effectiveness of $n = 3$ fields, no suppression was observed in either limited or diverted plasma targets with $n = 1$ fields. Recent experiments have also studied the variation in RMP RE suppression effectiveness with time of field application. No suppression was observed if the RMP was applied after the TQ was complete, while the suppression statistics illustrated in figure 16 correspond to pre-TQ application of the field. One conclusion of these studies is that the RMP is incapable of deconfining RE from the mature current channel. However, the successful suppression by pre-TQ field application suggests that the RMP affects the seed deconfinement that occurs in the TQ, perhaps by altering the nature of the MHD activity. Since heat losses during the TQ is dominated by open field line conduction, the degree of RE deconfinement by loss along open field lines during the TQ would be expected to correlate with post-TQ plasma impurity content since this produced by conducted heat load to the wall. Figure 17 shows the peak RE current amplitude plotted as a function of the CQ characteristic rate (inverse characteristic time of the decay) for a large ensemble of Ar pellet-induced

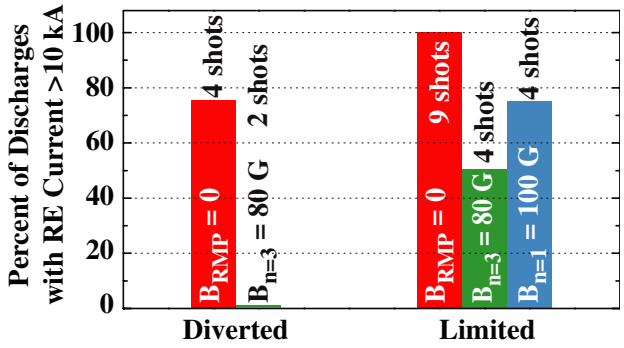

Figure 16. Statistical distribution of successful RMP suppression of post-disruption RE current for diverted and limited scenarios using different applied magnetic perturbations: $n = 3$ and $n = 1$.

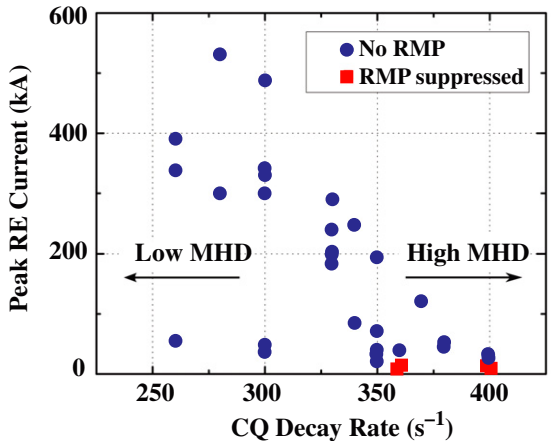

Figure 17. Peak RE current value as a function of the CQ characteristic decay rate for the non-RMP diverted cases (circles) and the RMP suppressed diverted case (square).

disruption diverted discharges. Four discharges with RMP suppression are also shown, corresponding to CQ rates among the highest in the dataset. The variation in RE current for the same current decay rates suggests variation in initial seed population, while the secular decline in maximum RE current with increasing initial CQ current decay rate is consistent with a speculated increase in open field line transport (induced by higher MHD activity) both deconfining more effectively the initial RE seed and generating higher localized convected heat flux to the wall thus higher impurity content during the disruption. This higher impurity content increases the post-TQ resistivity thus the I_p CQ decay rate. Further analysis will be required to establish whether effectiveness of RE deconfinement on open field lines is correlated with the nature of TQ MHD, and if RMP fields affect these instabilities so as to enhance the deconfinement.

5. Conclusion

The new SPI technique has shown promising results in terms of assimilation efficiency and deep penetration. The parameter scan has shown that a high initial flow rate is critical for the efficiency of the MGI technique (explaining also the higher efficiency of SPI because of its high flow rate). The SHPI technique shows promise but needs significant further study: the thickness of the wall has to be much thinner than previously estimated. The low elongation limited plasma target enabled the reliable generation of significant RE currents which allowed testing of mitigation techniques on an existing beam. The control of the RE position and amplitude by applied external fields has proven efficient and could allow easier mitigation by giving more time to apply other techniques. The RMP mitigation method of RE may have shown some efficiency probably related to an amplified MHD activity deconfining the RE seed prior to the CQ.

Acknowledgment

This work was partially supported by the Oak Ridge National Laboratory managed by UT-Battelle, LLC for the US Department of Energy under DE-AC05-00OR22725 and also supported under US/DOE under DE-FC02-04ER54698, DE-FG02-95ER54309 and DE-FG02-07ER54917.

References

[1] Hender T.C. *et al* 2007 *Nucl. Fusion* **47** S128
[2] Rosenbluth M.N. and Putvinsky S.V. 1997 *Nucl. Fusion* **37** 1355
[3] Wesley J.C. *et al* 2008 *Fusion Energy: Proc. 22nd IAEA Conf. (Geneva, Switzerland, 2008)* http://www-naweb.iaea.org/napc/physics/FEC/FEC2008/papers/ex_7-3rb.pdf
[4] Bozenkov S.A. *et al* 2008 *Plasma Phys. Control. Fusion* **50** 105007
[5] Pautasso G. *et al* 2007 *Nucl. Fusion* **47** 900
[6] Lehnen M., Bohzenkov S.A., Abdullaev S.S. and the TEXTOR Team 2008 *Phys. Rev. Lett.* **100** 255003-1
[7] Yoshino R. and Tokuda S. 2000 *Nucl. Fusion* **40** 1293
[8] James A.N. *et al* 2011 Pellet interaction with runaway electrons *J. Nucl. Mater.* submitted
[9] Hollmann E.M. *et al* 2005 *Nucl. Fusion* **45** 1046
[10] Combs S.K. *et al* 2010 *IEEE Trans. Plasma Sci.* **38** 400
[11] Commaux N., Baylor L.R., Jernigan T.C., Hollmann E.M., Parks P.B., Humphreys D.A., Wesley J.C. and Yu J.H. 2010 *Nucl. Fusion* **50** 112001
[12] Sovinec C.R. *et al* 2004 *J. Comput. Phys.* **195** 355
[13] Hollmann E.M. *et al* 2008 *Nucl. Fusion* **48** 115007
[14] Hollmann E.M. *et al* 2010 *Phys. Plasmas* **17** 056117
[15] Hollmann E.M. *et al* 2009 *Atomic Processes in Plasmas: Proc. 16th Int. Conf. (Monterey, CA, 2009)* vol 1161 p 65
[16] Ferron J.R., Walker M.L., Lao L.L., St John H.E., Humphreys D.A. and Leuer J.A. 1998 *Nucl. Fusion* **38** 1055
[17] Humphreys D.A. *et al* 2009 *Nucl. Fusion* **49** 115003
[18] Izzo V.A. *et al* 2010 *Fusion Energy: Proc. 23rd Int. Conf. (Daejeon, South Korea, 2010)* (Vienna: IAEA) http://www-pub.iaea.org/MTCD/Meetings/PDFplus/2010/cn180/cn180_papers/ths_9-2.pdf
[19] Kadomtsev B.B. 1984 *Plasma Phys. Control. Fusion* **26** 217